SINTEF
PROCEEDINGS
2

Proceedings of the 12th International Conference on Computational Fluid Dynamics in the Oil & Gas, Metallurgical and Process Industries

Progress in Applied CFD – CFD2017

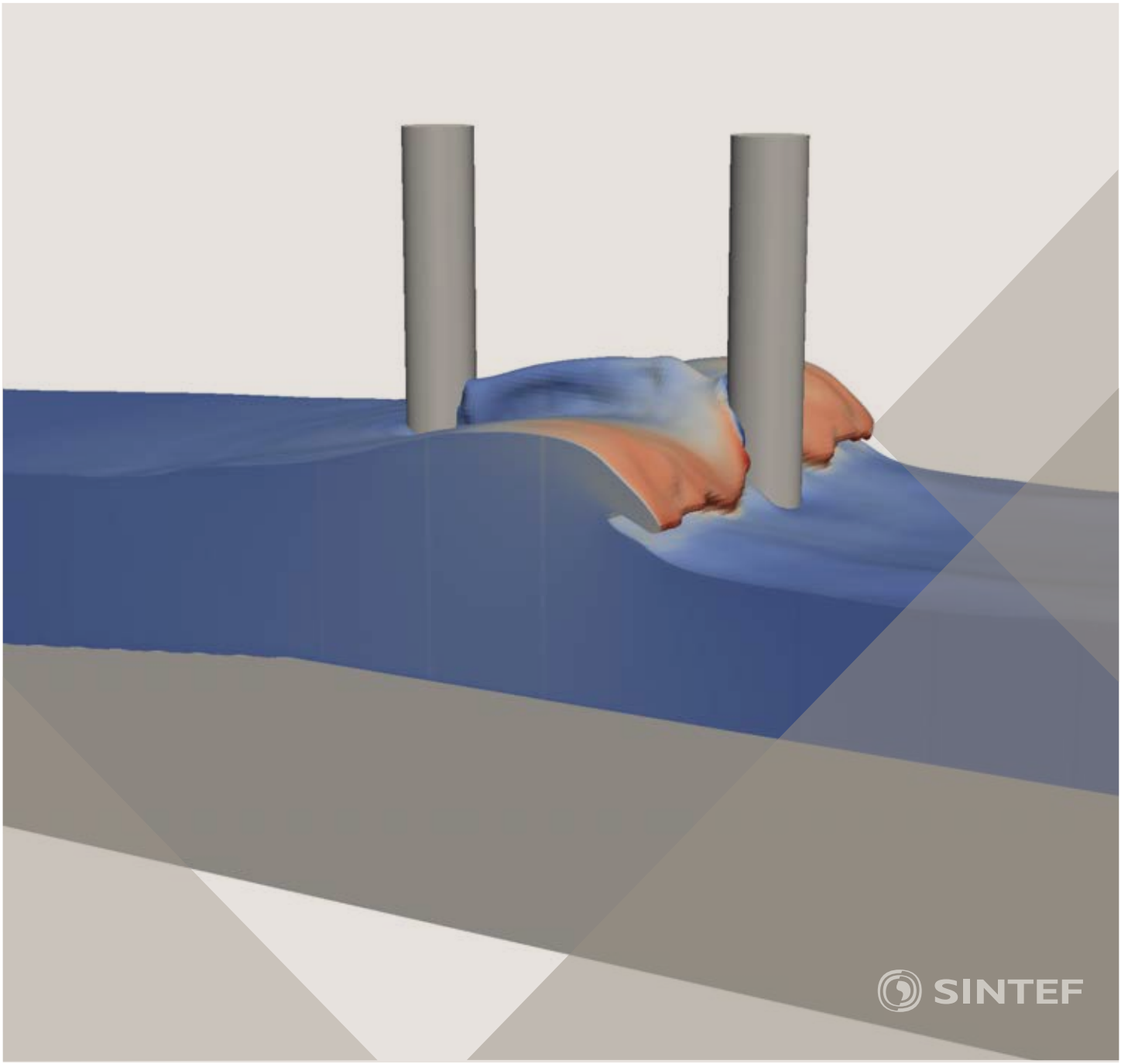

SINTEF Proceedings

Editors:
Jan Erik Olsen and Stein Tore Johansen

Progress in Applied CFD – CFD2017

Proceedings of the 12th International Conference on Computational Fluid Dynamics in the Oil & Gas, Metallurgical and Process Industries

SINTEF Academic Press

SINTEF Proceedings no 2
Editors: Jan Erik Olsen and Stein Tore Johansen
Progress in Applied CFD – CFD2017
Selected papers from 10th International Conference on Computational Fluid Dynamics in the Oil & Gas, Metallurgical and Process Industries

Key words:
CFD, Flow, Modelling

Cover, illustration: Arun Kamath

ISSN 2387-4295 (online)
ISBN 978-82-536-1544-8 (pdf)

© Copyright SINTEF Academic Press 2017
The material in this publication is covered by the provisions of the Norwegian Copyright Act. Without any special agreement with SINTEF Academic Press, any copying and making available of the material is only allowed to the extent that this is permitted by law or allowed through an agreement with Kopinor, the Reproduction Rights Organisation for Norway. Any use contrary to legislation or an agreement may lead to a liability for damages and confiscation, and may be punished by fines or imprisonment

SINTEF Academic Press
Address: Forskningsveien 3 B
PO Box 124 Blindern
N-0314 OSLO
Tel: +47 73 59 30 00
Fax: +47 22 96 55 08

www.sintef.no/byggforsk
www.sintefbok.no

SINTEF Proceedings
SINTEF Proceedings is a serial publication for peer-reviewed conference proceedings on a variety of scientific topics.
The processes of peer-reviewing of papers published in SINTEF Proceedings are administered by the conference organizers and proceedings editors. Detailed procedures will vary according to custom and practice in each scientific community.

PREFACE

This book contains all manuscripts approved by the reviewers and the organizing committee of the 12th International Conference on Computational Fluid Dynamics in the Oil & Gas, Metallurgical and Process Industries. The conference was hosted by SINTEF in Trondheim in May/June 2017 and is also known as CFD2017 for short. The conference series was initiated by CSIRO and Phil Schwarz in 1997. So far the conference has been alternating between CSIRO in Melbourne and SINTEF in Trondheim. The conferences focuses on the application of CFD in the oil and gas industries, metal production, mineral processing, power generation, chemicals and other process industries. In addition pragmatic modelling concepts and bio-mechanical applications have become an important part of the conference. The papers in this book demonstrate the current progress in applied CFD.

The conference papers undergo a review process involving two experts. Only papers accepted by the reviewers are included in the proceedings. 108 contributions were presented at the conference together with six keynote presentations. A majority of these contributions are presented by their manuscript in this collection (a few were granted to present without an accompanying manuscript).

The organizing committee would like to thank everyone who has helped with review of manuscripts, all those who helped to promote the conference and all authors who have submitted scientific contributions. We are also grateful for the support from the conference sponsors: ANSYS, SFI Metal Production and NanoSim.

Stein Tore Johansen & Jan Erik Olsen

Organizing committee:

Conference chairman: Prof. Stein Tore Johansen
Conference coordinator: Dr. Jan Erik Olsen
Dr. Bernhard Müller
Dr.Sigrid Karstad Dahl
Dr.Shahriar Amini
Dr.Ernst Meese
Dr.Josip Zoric
Dr.Jannike Solsvik
Dr.Peter Witt

Scientific committee:

Stein Tore Johansen, SINTEF/NTNU
Bernhard Müller, NTNU
Phil Schwarz, CSIRO
Akio Tomiyama, Kobe University
Hans Kuipers, Eindhoven University of Technology
Jinghai Li, Chinese Academy of Science
Markus Braun, Ansys
Simon Lo, CD-adapco
Patrick Segers, Universiteit Gent
Jiyuan Tu, RMIT
Jos Derksen, University of Aberdeen
Dmitry Eskin, Schlumberger-Doll Research
Pär Jönsson, KTH
Stefan Pirker, Johannes Kepler University
Josip Zoric, SINTEF

CONTENTS

MODELLING OF CHEMICAL REACTIONS IN METALLURGICAL PROCESSES

M. Efe KINACI[1]*, **Thomas LICHTENEGGER**[2,3]†, **Simon SCHNEIDERBAUER**[1]‡

[1]Christian Doppler Laboratory for Multi-Scale Modelling of Multiphase Processes, 4040 Linz, AUSTRIA

[2]Linz Institute of Technology (LIT), Johannes Kepler University, 4040 Linz, AUSTRIA

[3]Department of Particulate Flow Modelling, Johannes Kepler University, 4040 Linz, Austria

* E-mail: mustafa_efe.kinaci@jku.at
† E-mail: thomas.lichtenegger@jku.at
‡ E-mail: simon.schneiderbauer@jku.at

ABSTRACT

Iron-ore reduction has attracted much interest in the last three decades since it can be considered as a core process in steel industry. The iron-ore is reduced to iron with the use of blast furnace and fluidized bed technologies. To investigate the harsh conditions inside fluidized bed reactors, computational tools can be utilized. One such tool is the CFD-DEM method, in which the gas phase reactions and governing equations are calculated in the Eulerian (CFD) side, whereas the particle reactions and equation of motion are calculated in the Lagrangian (DEM) side. In this work, this method has been extended to cover the most common types of representation models for the reactions of solids submerged in fluids. These models are the Shrinking Particle Model (SPM) and the Unreacted Shrinking Core Model (USCM). With the use of the SPM, the implemented communication framework between the CFD and DEM sides have been verified by running some preliminary cases and comparing the species mass balances. In the modelling of iron-oxide reduction the SPM is insufficient to represent the different reaction steps, therefore a three-layered USCM is utilized. The implemented USCM is validated by running some preliminary cases.

Keywords: CFD-DEM, iron-ore reduction, chemical models, particle shrinkage, unreacted-core model .

INTRODUCTION

The rising energy demands, the deterioration of the quality of ore and coal due to high costs and low availability related with the shortage of resources, as well as the increased usage of mini mills, which might replace the conventional route of steel-making with the use of scrap or scrap substitutes, has lead to the development of new ways for the direct reduction of iron ores (Habermann *et al.*, 2000; Yang *et al.*, 2010). The practical importance of being used as feedstock in iron- and steel-making processes has also played a role at encouraging researchers to give attention to the reduction of iron-oxides (Donskoi and McElwain, 2003; Turkdogan and Vinters, 1971). Currently, the three available iron-making technologies are the blast furnace, smelting reduction and direct reduction technologies.

The leading process used in iron-making is the blast furnace, which consists of a moving bed reactor with countercurrent flow of the solid reactants against a reducing gas. In the blast furnace process, the iron ore fines which built up around 80% of iron ores, need to go through a pelletizing or sintering process (Schenk, 2011). In some cases, fine ores can directly be charged into the reduction process such as the fluidized bed technology, making it highly advantageous. Such fluidized bed reactors are used in the pre-reduction stage of the FINEX® process (Habermann *et al.*, 2000; Primetals, 2015). The FINEX® process produces hot metal in the same quality as traditional blast furnaces, however the coke making and sintering of the fine ores are avoided. The iron-ores that are charged into the process go through fluidized bed reactors where they are heated and reduced to DRI (Direct Reduced Iron), which is charged into the melter gasifier where final reduction and melting as well as the production of reducing gas by gasification of coal with oxygen takes place. Another advantage of the FINEX® process is the exhaust gas, which can be used for various other applications such as heating within a steel plant, power generation and so forth (Plaul *et al.*, 2009).

The main reactions for the reduction of metallic oxide with a gaseous reductant of carbon monoxide (CO) and hydrogen (H_2) can be expressed with the following steps:

Hematite to Magnetite:

$$3\,Fe_2O_3 + CO/H_2 \longrightarrow 2\,Fe_3O_4 + CO_2/H_2O \qquad (1)$$

Magnetite to Wustite:

$$Fe_3O_4 + CO/H_2 \longrightarrow 3\,FeO + CO_2/H_2O \qquad (2)$$

Wustite to Iron:

$$FeO + CO/H_2 \longrightarrow Fe + CO_2/H_2O \qquad (3)$$

If the reaction temperature is below $570^{\circ}C$, then there is no wustite formation and magnetite reduces directly to metallic iron with the reaction

$$\frac{1}{4}Fe_3O_4 + CO/H_2 \longrightarrow \frac{3}{4}Fe + CO_2/H_2O \qquad (4)$$

The carbon monoxide that is utilized in the indirect reduction of iron-oxide comes from the gasification of carbon with carbon-dioxide that is described with the homogeneous, endothermic Boudouard reaction (5) and from the water-gas reaction (6), which can be defined as

$$CO_2 + C \longrightarrow 2\,CO, \qquad (5)$$

$$C + H_2O \longrightarrow CO + H_2. \qquad (6)$$

Since access to the reactor is limited due to harsh conditions inside, carrying out measurements to investigate the processes is complicated. Thus, in order to better understand the

reactors and to make improvements on the processes, simulation methods and computational tools are utilized. One such tool is the Two-Fluid Model (TFM), which is an Euler-Euler approach that treats the solid and the fluid phases as a continuum. However, this model lacks the proper representation of particle size description and the related physical phenomena. In order to represent micro-scale phenomena, the TFM would require a fine spatial grid and that would make the process unaffordable for industrial scale utilization. If a coarse-graining is carried out there would be a loss of unresolved (small) scales and lead to errors (van der Hoef *et al.*, 2006; Schneiderbauer and Pirker, 2014). Another tool uses the coupling of CFD (Computational Fluid Dynamics) for the continuous fluid phase (i.e. the reduction gas) and the DEM (Discrete Element Method) for the discrete particles such as iron-ore and coal. These methods are coupled in a CFD-DEM approach based on the open source software packages OpenFOAM (OpenCFD Ltd. 2009) and LIGGGHTS (LIGGGHTS, 2011). DEM provides an easier way to evaluate the per-particle chemistry such as the shrink/growth of particles due to reactions and it does not require to transfer these reactions to a continuum representation. However, to tackle industrial scale operations with the CFD-DEM a coarse-graining needs to be carried out in order to reduce the computational demands, which is an upcoming investigation of this research. Another method that can be thought of would be the hybrid Lagrangian-Eulerian model that combines the Lagrangian discrete phase model (DPM) and a coarse-grained two-fluid model (TFM) such as in the works of (Schneiderbauer *et al.*, 2016).

MODELLING OF IRON-ORE REDUCTION

An effective investigation of iron-ore reduction needs to consider the thermodynamic aspects of the reduction reaction such as the conditions required for the reaction to take place or even if it is possible for the reaction to occur, as well as the kinetic aspects such as the reaction rates and concentration changes (Schmidt, 1998).

Thermochemical Aspects

In chemical reactions, spontaneity defines if the reaction occurs without being driven by an outside force. If a reaction is spontaneous the entropy of the reaction increases, and it can be considered that the system is able to release its *free energy* and move to a more stable state. The free energy is the part of the total enthalpy that can be converted into useful work. The free energy, just like enthalpy, cannot be measured by itself. However, the change of free energy can be calculated with

$$\Delta G_T^\circ = \Delta H_T^\circ - T\Delta S_T^\circ. \tag{7}$$

The change of free energy of a system is at its minimum value, if the system is in an equilibrium. The values for the standard free energies can be found in the thermodynamic data tables available in literature's from (Von Bogdandy and Engell, 2013), (Turkdogan, 1980) , and the JANAF-Thermochemical tables. An error, no matter how small, in the value of ΔG leads to a great amount of change in the shape of the equilibrium curves in an equilibrium phase diagram (Von Bogdandy and Engell, 2013). The chemical equilibrium can be defined with the equilibrium constants of the reaction. The various correlations defining the equilibrium constants can help to define the stability areas for the different iron oxides depending on temperature and composition of the reducing gas. The equilibrium constants can be considered as the ratio of molar concentrations of products to the reactants such as in the case of a general reaction $aA + bB \longrightarrow cC + dD$, the equilibrium constant can be defined as

$$K_c = \frac{[C]^c[D]^d}{[A]^a[B]^b} \tag{8}$$

or with the standard free energy change as (Levenspiel, 1999)

$$lnK = \frac{-\Delta G^\circ}{RT}. \tag{9}$$

An equilibrium phase diagram for the thermodynamically stable phases that occur in the reduction of iron-oxide to metallic iron is one of the most useful phase diagrams in the reduction process. One such diagram demonstrates the reduction processes of the iron-oxygen-carbon system, which is also called the *Baur-Glaessner Diagram*. In this diagram, as it is demonstrated in Fig. 1, the stabilities for the iron-oxides and iron phases are depicted as a function of temperature and CO/CO_2 mixture with the available correlations for the equilibrium constant from literature and the ones calculated.

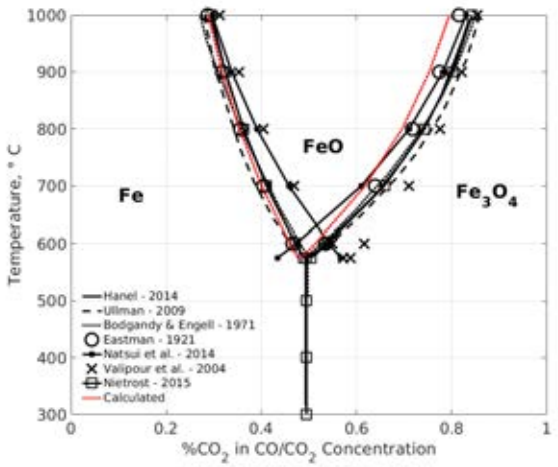

Figure 1: Equilibrium gas composition depending on the temperature for the iron-oxygen-carbon system at 1 atmospheric pressure.

The concentration molar fraction of the relative gas species can be determined with the use of the equilibrium constant as

$$\frac{x_{CO_2}^{eq}}{x_{CO}^{eq}} = Ke_{\mathrm{Fe_xO_y,CO}}, \tag{10}$$

thus the molar fraction of the mixture can be defined with,

$$x_{CO_2}^{eq} = k_c \frac{Ke_{\mathrm{Fe_xO_y,CO}}}{1 + Ke_{\mathrm{Fe_xO_y,CO}}} \tag{11}$$

or

$$x_{CO}^{eq} = k_c \frac{1}{1 + Ke_{\mathrm{Fe_xO_y,CO}}}, \tag{12}$$

in which k_c represents the total content of carbon in the system that can be expressed with

$$x_{CO}^{eq} + x_{CO_2}^{eq} = k_c. \tag{13}$$

As a more advanced method one might consider a four-component gas mixture of CO, H_2, CO_2 and H_2O to be represented in a single Baur-Glaessner Diagram with an abscissa of $CO + H_20$ or $H_2 + CO_2$ content.

Reaction Kinetics

To depict the progress of the fluid-solid reactions a model is chosen that is similar to reality. The most common types of representation models for the non-catalytic reactions of solids submerged in fluids is the shrinking particle model (SPM) and the unreacted shrinking core model (USCM) (Levenspiel, 1999).
In the SPM, only the surface of the particle is reacting with the surrounding fluid. In, this type of model there are no layer formations due to reaction and the products diffuse directly into gas. As the reaction progresses, the particle size shrinks and eventually disappears completely. In Fig. 2, the SPM is depicted, in which the particle shrinks and disappears with time.

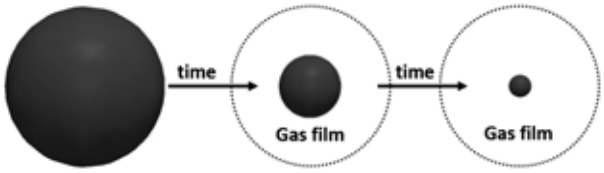

Figure 2: A schematic of the SPM, where the solid particle is reacting with the fluid without an ash layer formation.

The rate of change for the shrinkage/growth of a sphere can be expressed with (Levenspiel, 1999; Schmidt, 1998)

$$\frac{1}{4\pi R^2}\frac{dN_B}{dt} = \frac{b}{4\pi R^2}\frac{dN_A}{dt} = bkC_A \tag{14}$$

where k is the rate coefficient of surface reaction per unit area, C_A is the concentration of fluid species A at the surface of the particle, b is the stoichiometric coefficient for the reacting solid, N_B is the number of moles of solid B, which can be defined with

$$N_B = \frac{4\pi R^3 \rho_B}{3M_B} = \frac{m_B}{M_B}. \tag{15}$$

m_B is the mass of B, M_B is the molar mass of B, R is the radius of the particle, ρ_B is the density of solid particle. If we combine Eq. 14 and Eq. 15 than we can get for the rate of mass change for the gas species A as

$$\frac{dm_A}{dt} = k_g C_A M_A A_p. \tag{16}$$

The unreacted shrinking core model is one of the most precise models to represent the real-life fluid-solid reaction (Levenspiel, 1999; Homma *et al.*, 2005; Schmidt, 1998). The main reactions for the direct reduction of iron with a gaseous reductant can be expressed in three reaction steps with CO/H_2 reducing gas as shown in Reactions 1 - 4. The three layer unreacted shrinking core model developed by Philbrook, Spitzer and Manning (Tsay *et al.*, 1976) is able to represent the three interfaces of hematite/magnetite, magnetite/wustite and wustite/iron. An illustration of the model layer structure with corresponding radiuses, and a snapshot of a polished section of sintered hematite pellet that has been reduced 30% by H_2 is given as comparison to the USCM in Fig. 3.
The removal of oxygen follows these steps (Tsay *et al.*, 1976);

- The reducing gas is transported through the gas film onto the particle surface.

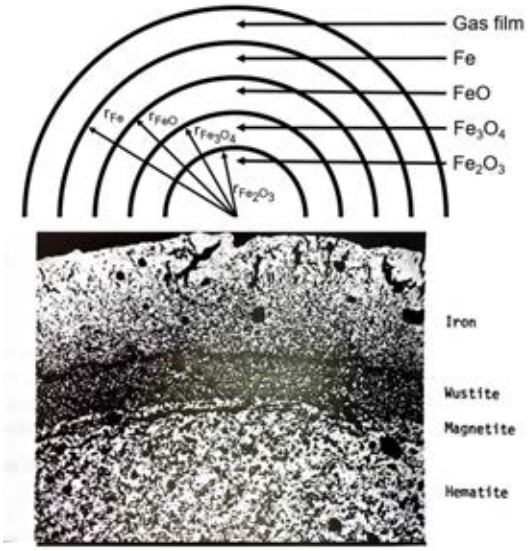

Figure 3: A schematic of the three layer unreacted shrinking core model (top) and a snapshot of a sintered pellet that has been reduced 30% (bottom) (Turkdogan, 1980).

- The reductant gas then diffuses through the porous iron layer.
- Part of the reductant reacts with wustite at the wustite/iron interface producing iron and gaseous product.
- Rest of the reducing gas diffuses through the wustite layer onto the wustite/magnetite interface.
- A portion of the gas reacts with magnetite at layer surface producing wustite and gaseous product.
- The balance gas diffuses through the magnetite layer onto the magnetite/hematite interface.
- Chemical reaction of the leftover gas occurs at the hematite core and produces magnetite and a gaseous product.
- The gaseous product diffuses outwards through the pores of the pellet.

Since each step is a resistance to the total reduction of the pellet, the reduction pattern of a single pellet can be considered to follow a resistance network such as an electrical resistance circuit network as illustrated in Fig. 4.

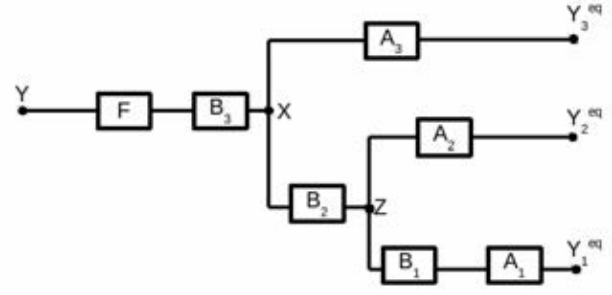

Figure 4: Resistance network diagram that illustrates the resistance of an iron-ore pellet that goes through in the reduction process.

The solution of this resistance network yields the reaction flow rate of $\dot{Y}_{j,i}$ of the gas species for the relative layers yields as;

- from hematite to magnetite as

$$\begin{aligned}\dot{Y}_{h,i} = &([A_3(A_2+B_2+B_3+F)+(A_2+B_2)(B_3+F)](Y-Y_1^{eq})\\ &-[A_3(B_2+B_3+F)+B_2(B_3+F)](Y-Y_2^{eq})\\ &-[A_2(B_3+F)](Y-Y_3^{eq}))\frac{1}{W_{3,i}},\end{aligned} \tag{17}$$

- from magnetite to wustite as

$$\begin{aligned}\dot{Y}_{m,i} = &([(A_1+B_1+B_2)(A_3+B_3+F)+A_3(B_3+F)](Y-Y_2^{eq})\\ &-[B_2(A_3+B_3+F)+A_3(B_3+F)](Y-Y_1^{eq})\\ &-[(A_1+B_1)(B_3+F)](Y-Y_3^{eq}))\frac{1}{W_{3,i}},\end{aligned} \tag{18}$$

- from wustite to iron as

$$\begin{aligned}\dot{Y}_{w,i} = &([(A_1+B_1)(A_2+B_2+B_3+F)+A_2(B_2+B_3+F)]\\ &(Y-Y_3^{eq})-[A_2(B_3+F)](Y-Y_1^{eq})\\ &-[(A_1+B_1)(B_3+F)](Y-Y_2^{eq}))\frac{1}{W_{3,i}}\end{aligned} \tag{19}$$

in which A_j represents the relative chemical reaction resistance term, B_j the relative diffusivity resistance term, j represents the layers hematite, magnetite and wustite and i the reducing gas species. F is the mass transfer resistance term, which is defined with $1/k_f.Y$ is the bulk gas mole fraction and Y_j^{eq} the relative layer equilibrium mole fractions. The denominator $W_{3,i}$ is expressed as

$$\begin{aligned}W = &[(A_1+B_1)(A_3(A_2+B_2+B_3+F)+(A_2+B_2)(B_3+F))\\ &+A_2(A_3(B_2+B_3+F)+B_2(B_3+F))].\end{aligned} \tag{20}$$

The chemical reaction resistance term $A_{j,i}$ can be expressed as

$$A_{j,i} = \left[\frac{1}{(1-f_j)^{\frac{2}{3}}}\frac{1}{k_j\left(1-\frac{1}{Ke_j}\right)}\right]_i \tag{21}$$

in which j represents the reduction layer, i the reducing gas, k the reaction rate constant and f_j is the local fractional reduction of the relative layer that is calculated as

$$f_j = 1-\left(\frac{r_j}{r_p}\right)^3. \tag{22}$$

The diffusivity resistance term $B_{j,i}$ can be calculated for the relative iron oxide component as (Valipour *et al.*, 2006; Valipour, 2009)

$$B_{h,i} = \left[\frac{(1-f_m)^{\frac{1}{3}}-(1-f_h)^{\frac{1}{3}}}{(1-f_m)^{\frac{1}{3}}(1-f_h)^{\frac{1}{3}}}\frac{r_g}{De_h}\right]_i, \tag{23}$$

$$B_{m,i} = \left[\frac{(1-f_w)^{\frac{1}{3}}-(1-f_m)^{\frac{1}{3}}}{(1-f_w)^{\frac{1}{3}}(1-f_m)^{\frac{1}{3}}}\frac{r_g}{De_m}\right]_i, \tag{24}$$

$$B_{w,i} = \left[\frac{1-(1-f_w)^{\frac{1}{3}}}{(1-f_w)^{\frac{1}{3}}}\frac{r_g}{De_w}\right]_i, \tag{25}$$

in which De_j represents the diffusion coefficient of the relative layer.
With the use of the reaction flow rate $\dot{Y}_{j,i}$ the relative mass flow rates of reactant gas between layers can be defined in a similar manner as in Eq. 16 with

$$\frac{dm_i}{dt} = C_i M_i A_p \dot{Y}_{j,i}. \tag{26}$$

Mass and Heat Transfer Coefficient

The mass transfer coefficient k_f which is used in the determination of the mass transfer term can be calculated through the Sherwood number or the Nusselt number as

$$\begin{aligned}Sh &= \frac{k_f d}{D_e},\\ Nu &= \frac{k_f}{k},\end{aligned} \tag{27}$$

where d is the diameter of pellet, D_e the diffusion coefficient and k the thermal conductivity. A number of correlations for determining the Sherwood number exist in literature. Lee and Barrow (Lee and Barrow, 1968) proposed a model through investigating the boundary layer and wake regions around the sphere leading to a Sherwood number of

$$Sh_t = (0.51Re^{0.5}+0.02235Re^{0.78})Sc^{0.33}, \tag{28}$$

where Sc stands for the Schmidt number and defined as $\frac{\nu}{\rho D}$. In more recent works from Valipour (Valipour, 2009) and Nouri et al. (Nouri *et al.*, 2011) the Sherwood and Nusselt numbers are expressed as

$$\begin{aligned}Sh &= 2+0.6Re^{0.5}Sc^{0.33},\\ Nu &= 2+0.6Re^{0.5}Pr^{0.33}.\end{aligned} \tag{29}$$

Pr represents the Prandtl number and is expressed as the specific heat times the viscosity over thermal conductivity $c\mu/k$.

Diffusivity Coefficient

Diffusivity of a gaseous species depends on properties such as the pore size distribution, void fraction and tortuosity. For example, according to (Tsay *et al.*, 1976) a pore size of 2μ to 5μ the Knudsen diffusion has been found to be 10 times faster than molecular diffusion, therefore in their work the Knudsen diffusion has been neglected and the effective binary gas diffusion was calculated with

$$[D_{j,i}]_{eff} = D_{j,i}\frac{\varepsilon}{\tau} \tag{30}$$

where ε represents the dimensionless void fraction, τ the tortuosity. (Valipour, 2009; Valipour *et al.*, 2006) has used the Fuller-Schettler-Giddings equation to determine the effective diffusivity as

$$D_{j,i} = \frac{10^{-7}T^{1.75}}{(P_t(\dot{v}_j^{1/3}+\dot{v}_i^{1/3}))^2}(\frac{1}{M_j}+\frac{1}{M_i})^{0.5} \tag{31}$$

in which the $\dot{v}$ is the diffusion volume of the relative species, M is the molecular weight, P_t the total flow pressure and T the temperature in Kelvin.

Reaction Rate Coefficient

For many reactions the rate expression can be expressed as a temperature-dependent term. It has been established that in these kinds of reactions, the reaction rate constant can be expressed with the Arrhenius' law (Levenspiel, 1999) as follows

$$k = k_0 \exp(\frac{-E_a}{RT}), \tag{32}$$

in which k_0 represents the frequency factor or the pre-exponential factor, E_a the activation energy, R the universal gas constant and T the temperature. The values for the pre-exponential factor and the activation energy can be found through various works (Tsay *et al.*, 1976; Valipour, 2009).

RESULTS

Firstly, the CFD-DEM coupling library is extended to cover the SPM, in which the particle reacts with the fluid without forming a layer. Afterwards with the use of the SPM, the communication framework between the Eulerian CFD side and the Lagrangian DEM side is verified.

A simple test case is developed, consisting of a single carbon particle that reacts with the reactant gas of O_2 with a user defined reaction rate constant. The communication of DEM and CFD works by first initializing the particles in the DEM side and transferring their information such as the locations and velocities onto the CFD side. This information is then used to localize the particles and determine the voidfraction, fluid density, temperature, drag force and the species concentration (mass fractions) at particle locations, which is communicated back to the DEM side. The newly transferred data is then used to determine the particle movement, the change in particle size and change of gas concentrations due to the chemical reactions for the new time step and is transferred back to CFD side. This process continues until a specified amount of time steps have been reached.

The test case results are verified by comparing the species mass balances. The particle only reacts with the O_2 present, and stops after the total amount of O_2 has been depleted. The mass change of the reactant and product gas species is investigated in relation to particle shrinking. The simulation results are compared with theoretical data that is calculated with the same species concentration as the simulation, which proves to be in a good agreement within. The mass of change of the gas species is illustrated depending on the time in Fig. 5.

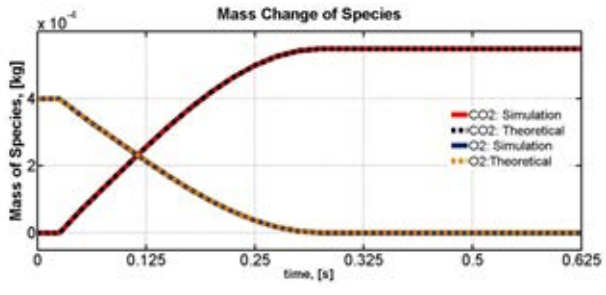

Figure 5: The change of mass of reacting gas species O_2 and product gas CO_2 depending on time.

After the communication framework is verified, the USCM is implemented into the DEM library. First, a correlation to determine the equilibrium constant $Ke_{Fe_xO_y}$ for every layer is implemented, and the relative equilibrium mole fractions of reactant and product gases are calculated as in Eq. 11 and 12. Therewith, the implemented reaction flow rates $\dot{Y}_{j,i}$, defined in Eq. 17 -19, are calculated and the mass flow rate of reactant gas between layers is determined. The mass flow rate of the reactant gas is used to calculated the mass transfer of every layer with the expression

$$\frac{dm_{B,l}}{dt} = \frac{dm_{A,l}}{dt} \frac{\upsilon_{B,l}}{\upsilon_{A,l}} \frac{M_{B,l}}{M_{A,l}}, \tag{33}$$

which is used to determine the radii of every iron-oxide layer. Since the model implemented at this time, only consider the chemical reaction resistance term $A_{j,i}$, only the reduction of layers for a single particle is investigated. Therefore, a preliminary test case is constructed that considers, just as in the SPM test case, a single particle, and the fractional reduction rate of every iron-oxide layer is investigated depending on time. An illustration of this reduction rate can be found in Fig. 6.

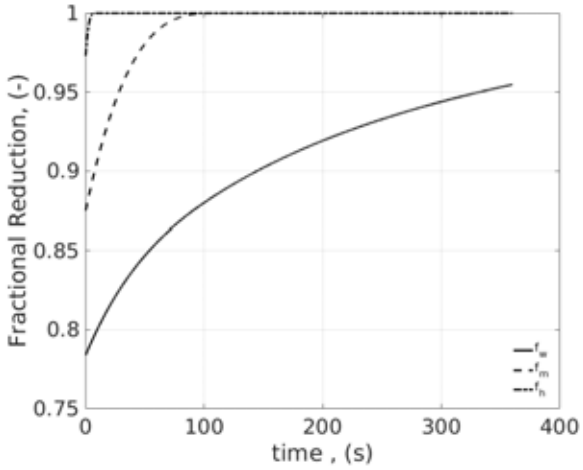

Figure 6: The fractional reduction of every iron oxide layer with time.

CONCLUSION AND OUTLOOK

In order to use the CFD-DEM method to investigate the reduction of iron-ore inside the fluidized bed reactors, the mathematical models representing the fluid-solid chemical reactions have been implemented into the DEM library. First, the SPM has been verified and used to test the communication framework between CFD and DEM sides. As these results were highly satisfactory, the framework is expanded to cover the three-layered USCM for a realistic representation of the iron-ore reduction. Since the investigation of the implemented model is still under way, some preliminary results from the shrinking of the layers of a single particle depending only on the chemical reaction resistance have been presented. For further research, valid correlations for the diffusion resistance term and the mass transfer term will be added to the DEM model. After the successful verification of the USCM with all its resistance terms is concluded, a coarse-graining of the CFD-DEM approach will be carried out and maybe a combination of the TFM and DPM for industrial scale simulations.

ACKNOWLEDGEMENTS

This work was funded by the Christian-Doppler Research Association, the Austrian Federal Ministry of Economy, Family and Youth, and the Austrian National Foundation

for Research, Technology and Development. The author also want to acknowledge the financial support from the K1MET center for metallurgical research in Austria (www.k1-met.com).

REFERENCES

DONSKOI, E. and MCELWAIN, D.L.S. (2003). "Estimation and modeling of parameters for direct reduction in iron ore/coal composites: Part I. Physical parameters". *Metallurgical and Materials Transactions B*, **34(1)**, 93–102.

HABERMANN, A., WINTER, F., HOFBAUER, H., ZIRNGAST, J. and SCHENK, J.L. (2000). "An Experimental Study on the Kinetics of Fluidized Bed Iron Ore Reduction". *ISIJ International*, **40(10)**, 935–942.

HOMMA, S., OGATA, S., KOGA, J. and MATSUMOTO, S. (2005). "Gas-solid reaction model for a shrinking spherical particle with unreacted shrinking core". *Chemical Engineering Science*, **60(18)**, 4971–4980.

LEE, K. and BARROW, H. (1968). "Transport processes in flow around a sphere with particular reference to the transfer of mass". *International Journal of Heat and Mass Transfer*, **11(6)**, 1013–1026.

LEVENSPIEL, O. (1999). *Chemical Reaction Engineering*.

NOURI, S.M.M., Ale Ebrahim, H. and JAMSHIDI, E. (2011). "Simulation of direct reduction reactor by the grain model". *Chemical Engineering Journal*, **166(2)**, 704–709.

PLAUL, F.J., BÖHM, C. and SCHENK, J.L. (2009). "Fluidized-bed technology for the production of iron products for steelmaking". *Journal of the Southern African Institute of Mining and Metallurgy*, **109(2)**, 121–128.

PRIMETALS (2015). "The finex process". Brochure. URL `http://primetals.com/en/technologies/ironmaking/finex%C2%AE/Lists/FurtherInformation/The%20Finex%20process.pdf`.

SCHENK, J.L. (2011). "Recent status of fluidized bed technologies for producing iron input materials for steelmaking". *Particuology*, **9(1)**, 14–23.

SCHMIDT, L.D. (1998). "The engeenering of chemical reactions". 536.

SCHNEIDERBAUER, S., PIRKER, S., PUTTINGER, S., AGUAYO, P., TOULOUPIDIS, V. and Martínez Joaristi, A. (2016). "A Lagrangian-Eulerian Hybrid Model for the Simulation of Poly-disperse Fluidized Beds: Application to Industrial-scale Olefin Polymerization". *submitted to Powder Technology*. URL `http://dx.doi.org/10.1016/j.powtec.2016.12.063`.

SCHNEIDERBAUER, S. and PIRKER, S. (2014). "Filtered and Heterogeneity-Based Subgrid Modifications for Gas-Solid Drag and Solid Stresses in Bubbling Fluidized Beds". *American Institute of Chemical Engineers*, **60(3)**, 839–854.

TSAY, Q.T., RAY, W.H. and SZEKLEY, J. (1976). "The modeling of hematite reduction with hydrogen plus carbon monoxide mixture". *AIChE J*, **22(6)**, 1064–1076.

TURKDOGAN, E. and VINTERS, J. (1971). "Gaseous reduction of iron oxides: Part I. Reduction of hematite in hydrogen". *Metallurgical Transactions*, **2(11)**, 3175–3188.

TURKDOGAN, E.T. (1980). "Physical chemistry of high temperature technology".

VALIPOUR, M.S. (2009). "Mathematical Modeling of a Non-Catalytic Gas-Solid Reaction : Hematite Pellet Reduction with Syngas". *Chemical Engineering*, **16(2)**, 108–124.

VALIPOUR, M.S., HASHEMI, M.Y.M. and SABOOHI, Y. (2006). "Mathematical modeling of the reaction in an iron ore pellet using a mixture of hydrogen, water vapor, carbon monoxide and carbon dioxide: an isothermal study". *Advanced Powder Technology*, **17(3)**, 277–295.

VAN DER HOEF, M.A., YE, M., van Sint Annaland, M., ANDREWS, A.T., SUNDARESAN, S. and KUIPERS, J.A.M. (2006). "Multiscale Modeling of Gas-Fluidized Beds". *Advances in Chemical Engineering*, **31**, 65–149.

VON BOGDANDY, L. and ENGELL, H.J. (2013). *The reduction of iron ores: scientific basis and technology*. Springer Science & Business Media.

YANG, K., CHOI, S., CHUNG, J. and YAGI, J.I. (2010). "Numerical Modeling of Reaction and Flow Characteristics in a Blast Furnace with Consideration of Layered Burden". *ISIJ International*, **50(7)**, 972–980.